### Title

TRANVIA (TVA) facilitates cellulose synthase trafficking and delivery to the plasma membrane




### Journal

Proceedings of the National Academy of Sciences of the United States of America, 118(30)

### ISSN

0027-8424



### Authors

Vellosillo, Tamara
Dinneny, José R
Somerville, Chris R
et al.



### Publication Date

2021-07-27

### DOI

10.1073/pnas.2021790118

Peer reviewed

# TRANVIA (TVA) facilitates cellulose synthase trafficking and delivery to the plasma membrane

Tamara Vellosillo[a,b,c,1], José R. Dinneny[c,1], Chris R. Somerville[a,1], and David W. Ehrhardt[b,c,1]

[a]Department of Plant and Microbial Biology, University of California, Berkeley, CA 94720; [b]Department of Plant Biology, Carnegie Institution for Science, Stanford, CA 94305; and [c]Department of Biology, Stanford University, Stanford, CA 94305

Contributed by Chris R. Somerville, June 8, 2021 (sent for review October 18, 2020; reviewed by Eric Nielsen and Georgia Drakakaki)

**Cellulose is synthesized at the plasma membrane by cellulose synthase (CESA) complexes (CSCs), which are assembled in the Golgi and secreted to the plasma membrane through the *trans*-Golgi network (TGN) compartment. However, the molecular mechanisms that guide CSCs through the secretory system and deliver them to the plasma membrane are poorly understood. Here, we identified an uncharacterized gene, *TRANVIA* (*TVA*), that is transcriptionally coregulated with the *CESA* genes required for primary cell wall synthesis. The *tva* mutant exhibits enhanced sensitivity to cellulose synthesis inhibitors; reduced cellulose content; and defective dynamics, density, and secretion of CSCs to the plasma membrane as compared to wild type. TVA is a plant-specific protein of unknown function that is detected in at least two different intracellular compartments: organelles labeled by markers for the TGN and smaller compartments that deliver CSCs to the plasma membrane. Together, our data suggest that TVA promotes trafficking of CSCs to the plasma membrane by facilitating exit from the TGN and/or interaction of CSC secretory vesicles with the plasma membrane.**

cellulose synthase | secretory pathway | TGN | cell wall

Plant cell walls are dynamic structures surrounding the cell protoplast, composed of a complex network of polysaccharides, including cellulose, hemicelluloses, and pectin that are constantly remodeled during growth and development and in response to environmental cues (1, 2). Cellulose, a polymer of long unbranched β-1,4-linked glucan chains and the main load-bearing component of plant cell walls, is synthesized at the plasma membrane (PM) by protein complexes visualized in scanning electron microscopy as sixfold symmetrical rosettes and known as cellulose synthase complexes (CSCs) (3, 4). Cellulose synthase (CESA) proteins constitute the catalytic core of the complex, which are represented by 10 isoforms in *Arabidopsis thaliana* (5). Genetic and biochemical studies led to a heteromeric model of cellulose synthesis in which three distinct CESA proteins are necessary to form a functional complex; CESA1, CESA3, and CESA6-like proteins are required for primary cell wall CSCs, whereas CESA4, CESA7, and CESA8 are required for secondary cell wall synthesis in *Arabidopsis* (6–8). In addition to the CESAs, several proteins have been identified to be components of or associated with CSCs at the PM: the glycosylphosphatidylinositol-anchored protein COBRA and the endoglucanase KORRIGAN (KOR) are required for optimal cellulose synthesis (9, 10); and CELLULOSE SYNTHASE INTERACTIVE 1/POM2 (CSI1/POM2) and COMPANION OF CELLULOSE SYNTHASE (CC1 and CC2) proteins appear to be required for the association of CSCs with microtubules (11–14). However, the molecular mechanisms by which CSCs are assembled, directed and delivered to their sites of action at the PM, and the roles that these processes may play in regulating cellulose production and cell wall synthesis, remain unanswered questions.

Many of the major advances in the study of cellulose biosynthesis in recent years have been achieved due to the development of fluorescently tagged CESA proteins and to advances in live-cell imaging techniques that together have allowed visualization of CSC organization and dynamics in living cells as they synthesize cellulose (15). Live-cell imaging of fluorescently tagged CESAs has also provided insights into CSC trafficking. The CSCs have been detected in the Golgi apparatus, where they are assumed to be assembled (16–18). The Golgi-localized glycosyltransferases STELLO (STL1 and STL2) have recently been identified as regulators of CSC assembly in the Golgi (19). CSCs are then secreted to the PM through the *trans*-Golgi network/early endosome (TGN/EE) compartment, a dynamic sorting organelle that transports newly synthesized proteins en route to other cellular locations including the vacuole and the PM (20, 21). CESA proteins have been colocalized with the SNARE proteins SYP41, SYP42, and SYP61, and with the $H^+$-ATPase subunit a1 (VHA-a1), all proteins associated with the TGN (17, 18, 22, 23). Post-Golgi compartments containing CESA have been referred to collectively as small CESA compartments (SmaCCs) (18) or microtubule-associated CESA compartments (MASCs) (17). At least a portion of the SmaCCs/MASCs population has been observed directly to deliver CSCs to the PM, events which are targeted by the cortical microtubule cytoskeleton (18). Additionally, evidence for transient association of SmaCCs with the actin cytoskeleton has been observed (24). The actin cytoskeleton is responsible for the motility and cell-wide distribution of CSC-containing compartments required for global organization of CSCs at the PM, and recently myosin XI has been described to mediate CSC delivery to the PM (18, 24, 25).

Under conditions where cellulose synthesis is inhibited by drugs or under osmotic stress, organelles containing CESA accumulate along, and interact strongly with, cortical microtubules (14, 17, 18). Upon relief of osmotic stress, SmaCCs in this population of organelles were observed to deliver CSCs to the PM (18), indicating that at least some of these compartments

## Significance

Cellulose, the most abundant biopolymer on Earth, is synthesized at the plasma membrane by cellulose synthase complexes (CSCs). The trafficking and delivery of CSCs from the Golgi apparatus to the plasma membrane is critical to maintain the level of cellulose synthesis in plants. We identified a plant-specific protein called TRANVIA (TVA) as a new component of CSC secretory compartments involved in the delivery of CSCs into the plasma membrane. This work reveals that CSCs require specific trafficking partners to facilitate their proper delivery, thus highlighting a new point at which this important process is regulated.

Author contributions: T.V., J.R.D., C.R.S., and D.W.E. designed research; T.V. and D.W.E. performed research; T.V. and D.W.E. analyzed data; and T.V., J.R.D., C.R.S., and D.W.E. wrote the paper.

Reviewers: E.N., University of Michigan; G.D., University of California, Davis

The authors declare no competing interest.



[1]To whom correspondence may be addressed. Email: tamarav@stanford.edu, dinneny@stanford.edu, crs@berkeley.edu, or ehrhardt@stanford.edu.

This article contains supporting information online at https://www.pnas.org/lookup/suppl/doi:10.1073/pnas.2021790118/-/DCSupplemental.

Published July 21, 2021.

associated with cortical microtubules during cellular stress are functional secretory vesicles. Probes for other PM proteins (BRI1, t-SNARE NPSN12) failed to show microtubule association and accumulation when cellulose synthesis was inhibited or osmotic stress was imposed (18); thus it is hypothesized that the SmaCCs associated with CSC delivery may represent a specialized secretory pathway involved in cell wall biosynthesis.

Recently, the exocyst complex, together with CSI1/POM2 and the protein PATROL1 (PTL1), which was first identified by its role in the trafficking of the $H^+$-ATPase AHA1, have been implicated in the delivery of CSCs to the PM (26). These investigators presented a timeline of events during CSC exocytosis where CESA and CSI1/POM2 appear first at the PM, followed by the tethering of these CSC-containing vesicles that are accompanied by the appearance of Sec5B and PTL1 (26). Furthermore, two PM-localized proteins have been identified, SHOU4 and SHOU4L, that directly interact with CESAs and negatively affect CSC exocytosis (27). However, the specific mechanisms that help convey CSCs from the Golgi to the PM are unknown and no proteins other than those that are part of the CSC cargo have been identified in the CSC delivery vesicles prior to arrival at the cell membrane.

Here, we identified TRANVIA (TVA) as a protein that facilitates trafficking of CSCs to the PM to support cellulose biosynthesis. TVA was identified through coexpression studies with genes encoding primary cell wall CESA isoforms (*CESA1*, *3*, and *6*), and plants bearing loss-of-function alleles have cellulose-related phenotypes and defects in CSCs secretion and activity at the PM. TVA protein colocalizes with CESA proteins at the TGN compartment and also at the secretory vesicles that deliver CSCs to the PM. Thus, we present a plant-specific protein that contributes to the cellulose synthesis pathway by promoting the secretion of CSCs from the Golgi to the PM.

## Results

**The *tva* Mutant Has Enhanced Sensitivity to Cellulose Synthesis Inhibitors and Reduced Cellulose Content.** To identify new proteins required for cellulose biosynthesis, we performed an analysis of coexpression with cellulose synthase (*CESA*) genes involved in primary cell wall biosynthesis (*SI Appendix*, Fig. S1*A*). Using the web tool GeneCAT (28), we identified a plant-specific gene that was coexpressed with the isoforms CESA1, 3, and 6, a gene we here term *TRANVIA* (*TVA*; At3g15480). *TRANVIA* encodes a predicted protein of 175 amino acids (aa) containing a Domain of Unknown Function (DUF1218) that defines a family of land plant proteins that feature a series of conserved cysteine residues (*SI Appendix*, Fig. S2*A*). TVA protein is predicted to be an integral membrane protein with three to four transmembrane domains (*SI Appendix*, Fig. S2*B*) (29). None of the genes in the TVA family has yet been assigned a biological function. Quantification of *TVA* transcript levels and analysis of transgenic *Arabidopsis* plants expressing the *β-glucuronidase* (*GUS*) reporter gene under the control of the 1.4-kb *TVA* promoter confirmed the coexpression analysis with primary wall *CESA* genes (*SI Appendix*, Fig. S1 *B–M*). Similar to *CESA1*, *3*, and *6* expression patterns (11, 30), GUS activity was observed in seedlings, root vasculature, and in rapidly elongating cells in etiolated seedlings (*SI Appendix*, Fig. S1 *C–G*). In addition, the *TVA* promoter drives GUS expression in floral tissues, rosette leaves, trichomes, and stomata (*SI Appendix*, Fig. S1 *H–M*).

To investigate whether mutations in the *TVA* gene cause defects in plant growth, we analyzed a homozygous T-DNA insertion line for this gene (*tva-1*, SALK_129213), in which *TVA* expression was highly reduced, as detected by qRT-PCR (*SI Appendix*, Fig. S3 *A* and *B*). Under standard growth conditions on agar plates or in soil, the *tva-1* mutant did not show any obvious alteration or defect in development compared to wild-type plants (Fig. 1 *A* and *C*). Since primary wall cellulose-deficient mutants typically display increased sensitivity to inhibitors of cellulose synthesis (3, 7, 14), we tested the sensitivity of the *tva-1* mutant to two such inhibitors, isoxaben and 2,6-dichlorobenzonitrile (DCB). The *tva-1* mutant was more sensitive to both drugs, showing 15% and 25% greater reduction in root length, respectively, compared with wild-type plants (Fig. 1 *A* and *B*). This increased sensitivity to both inhibitors was also observed in dark-grown *tva-1* seedlings (Fig. 1 *C* and *D*). The *tva-1* mutant phenotype was validated by the examination of a second T-DNA insertion line (GABI_256D04), in which the mutant allele was designated as *tva-2* (*SI Appendix*, Fig. S3 *A* and *B*). As with *tva-1*, this line displayed an increased sensitivity to both isoxaben and DCB treatments for root shortening (*SI Appendix*, Fig. S3 *C* and *D*). In addition to causing cell swelling and reduced organ growth, cellulose synthesis inhibitors have been shown to cause ectopic accumulation of lignin (31). The *tva* mutants showed excessive lignin staining compared to wild type in response to both inhibitors (*SI Appendix*, Fig. S3*E*), corroborating further their increased sensitivity to cellulose synthesis inhibition.

To test whether isoxaben and DCB sensitivity in *tva* mutants is due to a reduced level of cellulose, we performed a biochemical analysis of cell wall composition. These analyses revealed that the *tva-1* mutant has a significantly lower cellulose content relative to wild type, reduced by 20% in whole seedlings and stems, and ∼15% in hypocotyls and leaves (Fig. 1*E*). Other polysaccharides, neutral cell wall sugars, and uronic acids, exhibited minor changes compared with wild type (*SI Appendix*, Table S1). Taken together, our data indicate that the *tva-1* mutant is deficient in cellulose synthesis and/or content in plant cell walls.

**Dynamics, Delivery, and Density of CESA Complexes Are Affected in the *tva* Mutant.** To explore further the hypothesis that cellulose synthesis is negatively impacted by *TVA* loss of function, we assessed the distribution and dynamics of CESA complexes (CSCs) in the mutant background. A green fluorescent protein (GFP)-tagged CESA3 (7) was crossed into the *tva-1* mutant and visualized by spinning disk confocal microscopy. GFP-CESA3 labels subresolution particles at the PM that move at steady rates along roughly linear tracks in elongating hypocotyl cells (7, 15). The motility of CSCs at the PM is believed to be driven by the polymerization and extrusion of glucan chains into the cell wall, and it has been proposed to be a proxy for cellulose synthesis activity (15, 32). Thus, to evaluate CSC activity, we analyzed GFP-CESA3 velocity at the PM of etiolated hypocotyl cells from time-lapse images (Fig. 2*A* and Movie S1) (33). The analysis of these particles revealed a significant increase in the mean velocity of labeled particles in the *tva-1* mutant, 234 ± 109 nm/min, compared with the control where particles migrated with a speed of 205 ± 96 nm/min ($P < 0.001$, Student's *t* test; Fig. 2*B*). Thus, increased sensitivity to isoxaben and reduced cellulose content are not explained by reduced CSC activity. An alternative hypothesis is that fewer CSCs may be deployed in the cell membrane in *tva* mutants. Consistent with this possibility, time-averaged projections indicated that the GFP-CESA3 signal at the PM was reduced in the *tva-1* mutant as compared to wild type, despite their higher velocities (Fig. 2*A*). To probe this idea more directly, we measured the density of PM-localized GFP-CESA3 particles in both backgrounds. These analyses revealed that the density of labeled CSCs in etiolated hypocotyl cells of the *tva-1* mutant was in fact about 26% lower than in wild type (0.74 ± 0.02 CESA3 particles per square micrometer as compared to 1 ± 0.02 CESA3 particles per square micrometer, $P < 0.001$, Student's *t* test; Fig. 2*C*). This reduced density of CSCs in the mutant suggested a defect in either CSC secretion or internalization.

To assess if CESA secretion was reduced in the *tva-1* mutant, we quantified the rate of CSC delivery to the PM using a microscopic live-cell assay. Specifically, we photobleached a region of the cell cortex and counted the number of new CSCs that were delivered to this region over a fixed time interval as previously described (18). New CSC insertion events were identified by observing changes in the dynamics of newly arrived GFP-CESA3

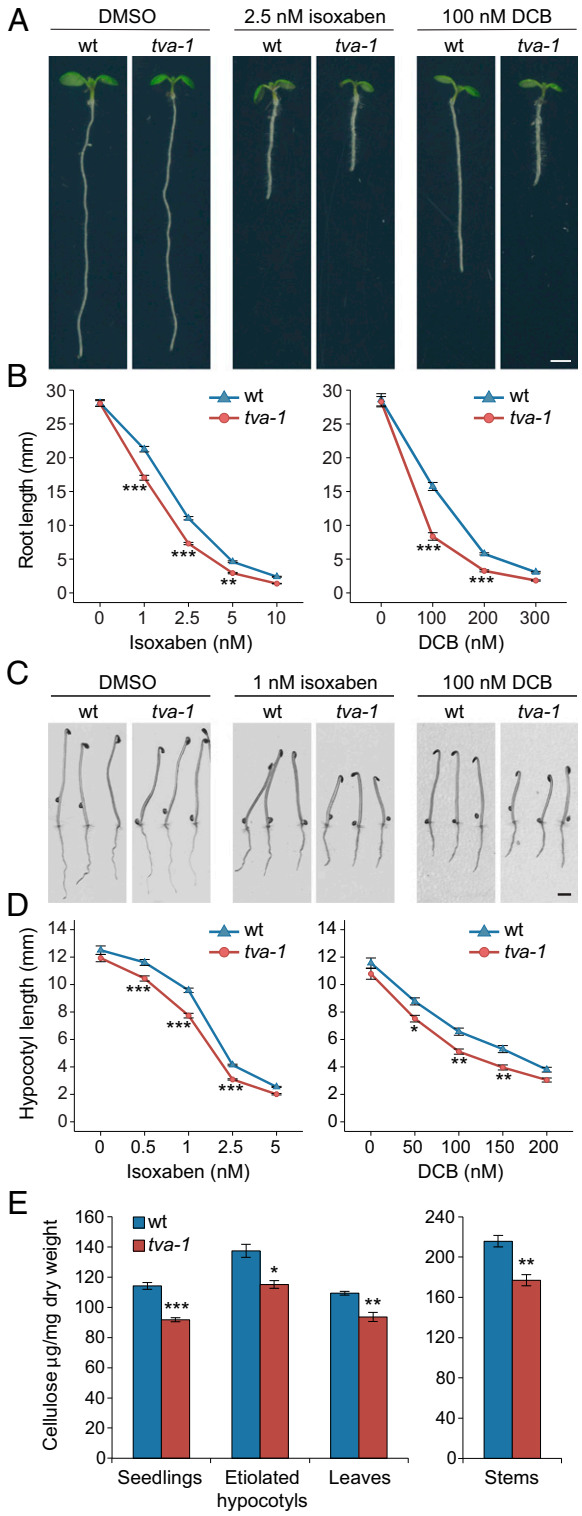


**Fig. 1.** The *tva* mutant exhibits an increased sensitivity to cellulose synthesis inhibition and a reduction in cellulose levels. (*A*) Seven-d-old Col-0 and *tva-1* mutant seedlings grown on half-strength MS media supplemented with 2.5 nM isoxaben and 100 nM DCB. (*B*) Bar graph of root length on media supplemented with increasing concentration of isoxaben (*Left*) or DCB (*Right*). (*C*) Four-d-old Col-0 and *tva-1* mutant etiolated seedlings grown on half-strength MS media supplemented with 1 nM isoxaben and 100 nM DCB. (*D*) Bar graph of hypocotyl length on media supplemented with increasing concentration of isoxaben (*Left*) or DCB (*Right*). In *B* and *D*, values are mean (± SEM) from three biological replicates with more than 10 seedlings per replicate. $*P < 0.05$, $**P < 0.01$, $***P < 0.001$, two-way ANOVA comparing wild-type (WT) and control treatments. (*E*) Cellulose content of primary cell walls (10-d-old light grown seedlings, 5-d-old etiolated seedlings and leaves from 4-wk-old plants) and secondary cell walls (stems from 5-wk-old plants). Values are mean (± SEM) from at least three biological replicates. $*P < 0.05$, $**P < 0.01$, $***P < 0.001$, Student's *t* test. (Scale bars, 2 mm.)

particles at the cell cortex. As GFP-CESA3 vesicles approach the cell membrane, they show rapid and erratic trajectories that first become spatially stabilized, which we infer to be vesicle tethering, and then transition into slowly moving particles as the vesicles presumably fuse with membrane and CSCs commence cellulose synthesis (18). We measured the CSC secretion rate in wild-type cells to be 4.96 ± 0.12 CESA-complex delivery events per square micrometer per hour. In the *tva-1* mutant, the CSC secretion was significantly reduced to a rate of 3.57 ± 0.14 CESA-complex delivery events per square micrometer per hour, a reduction of ~28% ($P < 0.001$, Student's *t* test, Fig. 2 *D* and *E*). This 28% reduction in CSC delivery rate is consistent with the previously measured 26% reduction in CSC density and could quantitatively account for the difference, assuming the lifetimes of the complexes at the PM are the same in wild type and *tva-1* mutants. Assuming that CSC densities and lifetimes were at a steady state over the interval of measurement, we calculated CSC mean lifetime to be ~12.1 min in wild type (1 particle $\mu m^{-2}$/4.96 events $\mu m^{-2}\ h^{-1}$) and 12.4 min in the *tva-1* mutant (0.74 particles $\mu m^{-2}$/3.57 events $\mu m^{-2}\ h^{-1}$), confirming they are both similar. Taken together, these results suggested that *TVA* facilitates the secretion of CSCs to the PM.

**TVA Is Detected in at Least Two Mobile Intracellular Compartments Whose Movement Is Dependent on Actin Function.** CSC secretion appears to be consistent with canonical secretion via the Golgi apparatus based on observation of CSCs and fluorescently tagged CESAs in Golgi and the TGN (16–18) and the observation of vesicle-like bodies carrying YFP-labeled CESA to the PM (18). To investigate whether TVA is present in the secretory pathway, and where along this pathway it might act, a GFP tag was fused in frame to the C terminus of a genomic *TVA* fragment under the control of the native *TVA* promoter. This construct rescued the *tva-1* drug-sensitive phenotype, indicating the fusion protein is functional (*SI Appendix*, Fig. S4). Observation of epidermal cells in dark-grown hypocotyls by spinning disk confocal microscopy revealed that TVA-GFP was detected in, and localized to, distinct motile bodies and foci at the cell cortex, displaying a range of apparent sizes and dynamic behaviors as they moved through the cytoplasm (Fig. 3 *A* and *B* and Movie S2). Smaller bodies typically displayed more erratic patterns of movement. Some of them appeared suddenly in the focal plane as they arrived from deeper planes, moved slowly for a few frames, or stabilized in a fixed position before disappearing quickly. The movement of larger bodies was less erratic, with many moving slowly in the optical plane of the cell cortex for prolonged intervals and others moving quickly along with the streaming cytosol. In an effort to quantify these differences we partitioned TVA compartments into two size classes based on an apparent bimodality in the distribution of TVA-GFP signal area in background subtracted and thresholded images (Fig. 3 *B* and *C*). Bodies at or below 0.15 $\mu m^2$ in optical area were termed *small*-TVA compartments, while those above this threshold were termed *large*-TVA compartments. To determine whether the apparent association of compartment size and dynamic behavior was quantitatively robust, we tracked all detected bodies in defined regions of interest within six cells and plotted the mean velocity in a range of values for the particle intensity (a measure of compartment size). This analysis confirmed a relationship between compartment size and movement where large bodies

PLANT BIOLOGY

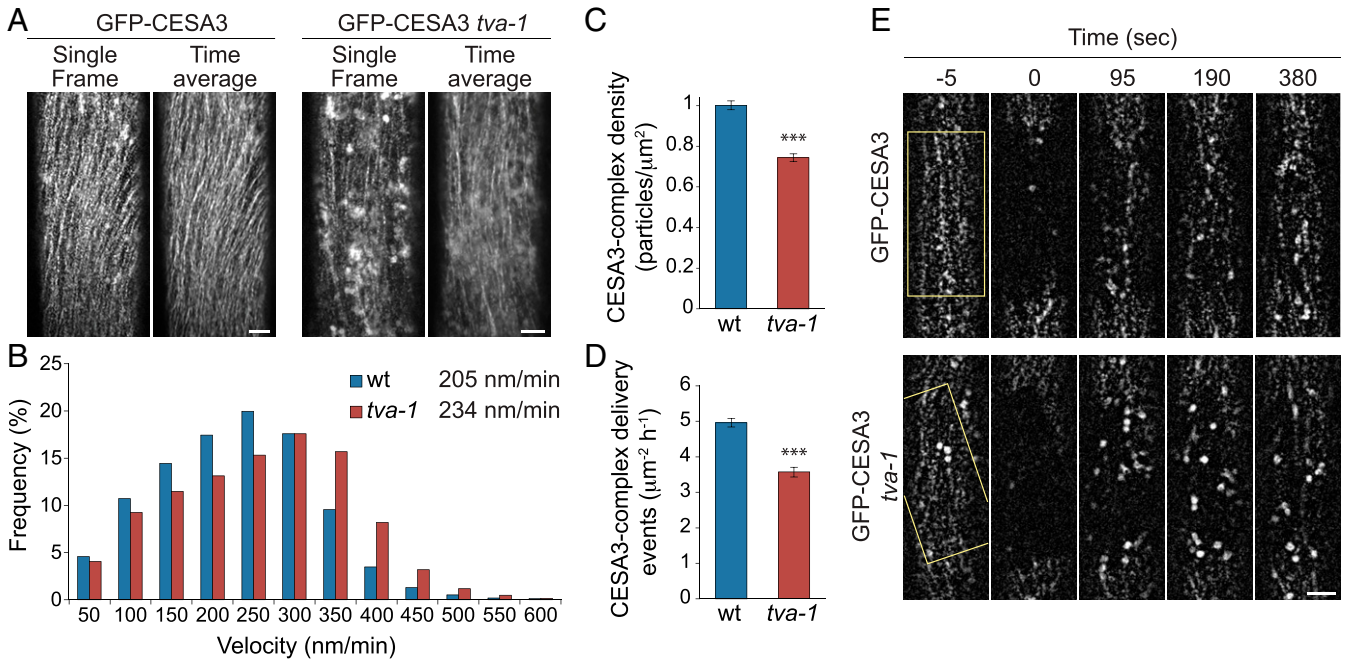


**Fig. 2.** GFP-CESA3 dynamics and trafficking are altered in the *tva-1* mutant. (*A*) Single-frame and time-averaged images (37 frames, 5-s interval) at the PM focal plane of 3-d-old etiolated wild-type (*Left*) and *tva-1* (*Right*) cells expressing GFP-CESA3. (*B*) Histogram of measured GFP-CESA3 particle velocities from at least 14 cells of six seedlings per genotype. Wild-type cells show a mean velocity of 205 nm/min, whereas particle velocity in the *tva-1* mutant is 234 nm/min ($P < 0.001$, Student's *t* test). (*C*) Graph displaying average density of GFP-CESA3 particles at the PM ($n = 16$ cells from eight seedlings per genotype). (*D*) Graph representing delivery events of CESA3 particles at the PM quantified from images captured after photobleaching a region of interest ($n = 20$ cells from six seedlings per genotype). Error bars represent SEM. ***$P < 0.001$, Student's *t* test. (*E*) Photobleaching of 3-d-old WT (*Upper*) and *tva-1* (*Lower*) etiolated hypocotyl cells expressing GFP-CESA3. The photobleached area is marked with a yellow rectangle. (Scale bars, 5 μm.)

tended to move more slowly and smaller bodies showed a greater range of velocities, from being static to having the highest velocities in the sample (Fig. 3*D*). These data suggest that TVA may be localized to at least two types of organelles with differences in size and motility, with *small*-TVA compartments showing a more heterogenous behavior (achieving either slow or very fast velocities).

Actin filaments are necessary for cytoplasmic streaming and are proposed to traffic membrane vesicles and their cargo (34, 35). To examine whether the motility or distribution of TVA-containing compartments is dependent on the organization of the actin cytoskeleton, we treated seedlings with the actin assembly inhibitor Latrunculin B (LatB). After treatment, the distribution of TVA compartments was disrupted with aggregates forming throughout the cytoplasm and beneath the PM (*SI Appendix*, Fig. S5*A* and Movie S3). Analysis of TVA compartment velocity and displacement after LatB treatment confirmed that their movement was highly reduced compared to control conditions (*SI Appendix*, Fig. S5*B*). To ask whether microtubule-directed motility may also play a role in TVA compartment motility, we depolymerized microtubules with oryzalin. This treatment caused a statistically significant reduction in compartment motility, but it was a small effect compared to that following LatB (*SI Appendix*, Fig. S5 *C* and *D* and Movie S4). These results suggest that TVA compartments are moving primarily via an actin-dependent mechanism, a conclusion also reached in previous studies for cellular compartments carrying CESA6 in unstressed conditions (15, 36).

**A *Large*-TVA Population Is Localized in the *Trans*-Golgi Network Compartment.** To investigate whether TVA compartments are part of the vesicle trafficking pathway, we treated etiolated seedlings expressing the TVA-GFP fusion with Brefeldin A (BFA), a fungal toxin that inhibits vesicular trafficking and results in the accumulation of endosomal and TGN membranes in so-called BFA compartments (37, 38). After BFA treatment, TVA-GFP accumulated in larger bodies, indicating that its localization is indeed BFA sensitive (Fig. 3*E*). Consistent with the idea that TVA bodies may be trafficking compartments, the endocytic tracer FM4-64, which progressively labels endosomes, the TGN, and the Golgi, showed colocalization with many TVA-GFP compartments after uptake for 6 min (Fig. 3*F*). Since compartments labeled by TVA-GFP were abundant and highly mobile, we performed a dynamic colocalization analysis to determine whether these observations could be a consequence of coincidental overlap. Colocalization was defined as cotranslation of overlapping signal in two channels over at least five frames of live-cell imaging. This analysis indicated that colocalization of TVA-GFP with FM4-64 endocytic compartments was observed overwhelmingly with the *large*-TVA compartments (83% colocalization; Fig. 3 *F* and *G* and Movie S5). We observed colocalization with *small*-TVA compartments more rarely, even after 20 min of the dye application (5% colocalization; Fig. 3 *F* and *G*). These observations suggest a functional distinction between the smaller and larger compartments; however, it is also possible that the amount of dye that may partition into the membranes of smaller compartments is below the limit of detection.

The presence of TVA-GFP bodies in BFA compartments and the early colocalization of larger TVA compartments with FM4-64 suggested that *large*-TVA compartments may be associated with either endosomes, the TGN compartment, and/or the Golgi. To assess these possibilities, we crossed known TGN and Golgi markers into the *tva-1* mutant expressing TVA-GFP. Dynamic colocalization analysis revealed a clear overlap of *large*-TVA with the two TGN markers: vacuolar ATPase subunit a1 (VHAa1)-mRFP (Fig. 4*A* and Movie S6) and mCherry-VTI12 SNARE protein (Fig. 4*A* and Movie S7) (39–42). Colocalization of all TVA-GFP compartments was close to 60% with both TGN markers, increasing to 85.9% and 81.4%, respectively, if we considered the *large*-TVA population alone (Fig. 4*B*). In addition, the analysis of

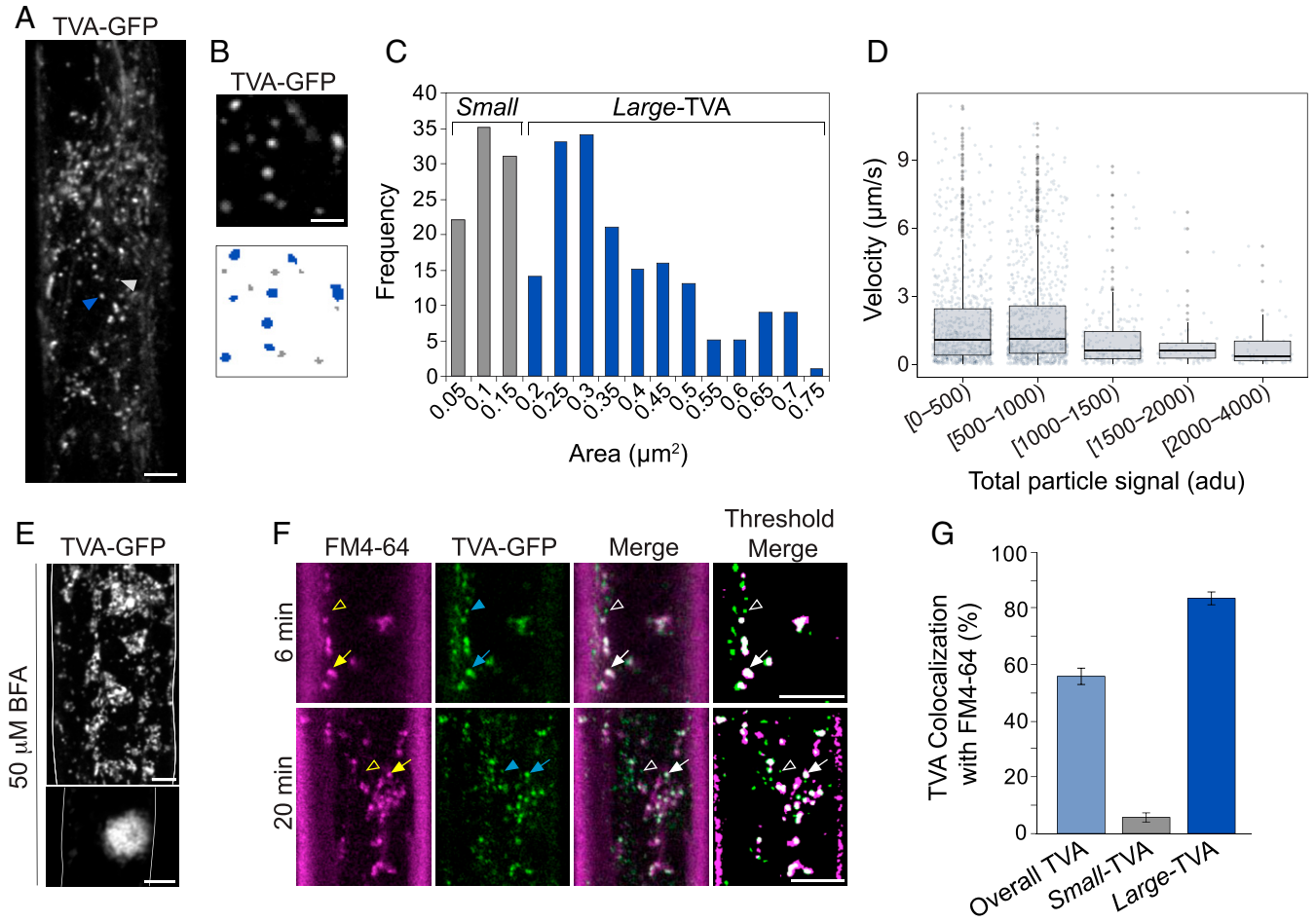


**Fig. 3.** TVA-GFP motile puncta are detected in two types of compartments with different size and motility, and one of them colocalizes with an endosomal compartment. (*A*) Single-frame image at the cell cortex focal plane of a 3-d-old etiolated hypocotyl cell expressing TVA-GFP under control of its own promoter. TVA-GFP is localized to larger (blue arrowhead) and smaller bodies (gray arrowhead). (*B*) Representative single frame (*Upper*) and thresholded image (*Lower*) used for particle size analysis. Larger and smaller bodies are colored in blue and gray, respectively. (*C*) Histogram showing the distribution of sizes of TVA-GFP compartments measured in 10 cells from three seedlings. Compartments at or below 0.15 μm$^2$ are termed *small*-TVA (gray bars), and those above are termed *large*-TVA (blue bars). (*D*) Boxplot showing the distribution of velocities of TVA-GFP compartments in different intervals of particle signal (arbitrary density units [adu]) measured in high-speed movies in 6 cells from three seedlings. (*E*) Single-frame images of 2 different cells expressing TVA-GFP showing different levels of BFA-body aggregation after exposure to 50 μM BFA for 2.5 h. (*F*) Single-frame images of cells expressing TVA-GFP that were incubated with 4 μM FM4-64 for 6 and 20 min (not BFA treated) and the thresholded merged image used for colocalization analyses. *Large*-TVA particles colocalize with endosomes stained by FM4-64 (filled arrows), whereas FM4-64 did not label *small*-TVA vesicles even after 20 min of incubation (arrowheads). (*G*) Percentage of overall TVA-GFP (light blue bar), *small*-TVA (gray bar), and *large*-TVA (dark blue bar) compartments that colocalize with FM4-64 for at least five contiguous frames of live-cell imaging. Dynamic colocalization was measured in 14 cells from four different seedlings (data are mean ± SEM). (Scale bars, 5 μm in *A*, *E*, and *F*; 2 μm in *B*.)

particle size for the TGN marker VHAa1-RFP revealed a similar distribution to *large*-TVA compartments (*SI Appendix*, Fig. S6). *Small*-TVA class bodies did not colocalize well with either marker (~6% colocalization for both markers; Fig. 4*B*), providing further support for the possibility that *small*-TVA compartments are functionally distinct from *large*-TVA compartments. By contrast to the TGN probes, the TVA-GFP signal displayed only minor overlap (~12% colocalization) with the Golgi marker mCherry-MEMB12 (Fig. 4 *A* and *B*) (40, 42); however, TVA compartments were often observed to cotranslate with the Golgi while tracking adjacently to them (Movie S8), consistent with previous observations of TGN dynamics in higher plants (20, 43, 44). Taken together, these data strongly suggest that many if not most *large*-TVA-GFP compartments are part of the TGN. Thus, one location where TVA may function is the TGN compartment. Alternatively, it could be loaded into vesicles at the TGN, where it functions further downstream.

**TVA Is Associated with CESA6 Proteins in the Secretion Pathway and during Their Delivery.** The localization of TVA in the secretory pathway, together with the observation that CESA density and delivery to the PM is lower in the *tva-1* mutant, suggested that TVA might play a role in the secretion of CSCs. To investigate whether the TVA protein is associated with primary CSCs, we generated lines expressing both TVA-GFP and tdTomato-CESA6 (tdT-CESA6) (24) and examined the dynamic colocalization of both proteins in etiolated hypocotyl cells (Fig. 5 *A* and *B*). This analysis revealed that 32.8% of the *large*-TVA compartments, and 10.9% of the *small*-TVA compartments, showed dynamic colocalization with tdT-CESA6–containing compartments at the cell cortex (Fig. 5*C*). However, we observed a large number of TVA-GFP particles that partially overlapped with large tdT-CESA6–labeled compartments, so we established a less strict overlapping criteria where both markers needed to be coincident with at least 15% of the total signal over five frames of live-cell imaging. An example of compartments fitting these

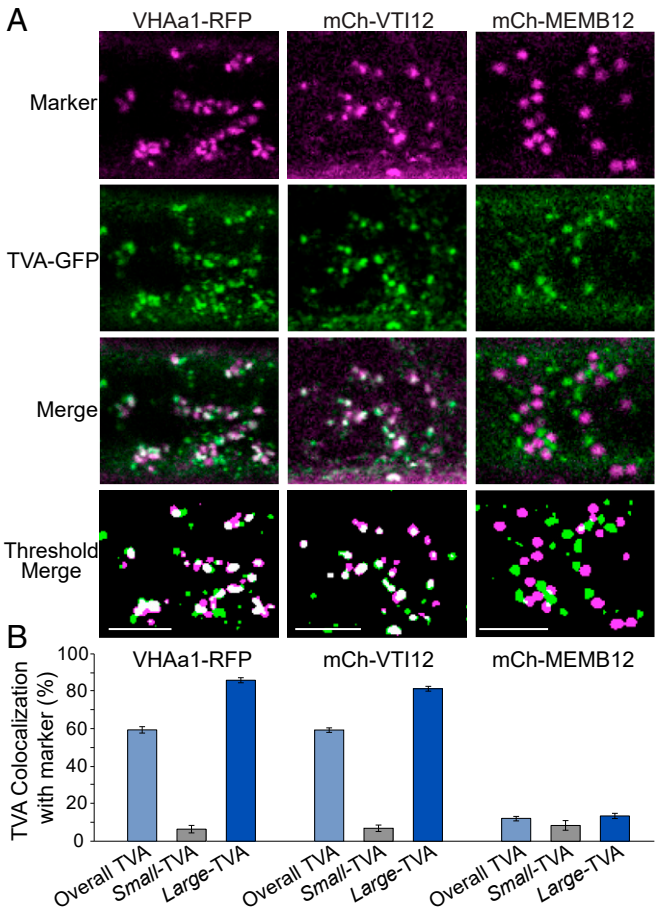


**Fig. 4.** The *large*-TVA population is localized to the TGN compartment. (*A*) Single-frame images of 3-d-old etiolated hypocotyl cells expressing both TVA-GFP and the TGN markers VHAa1-RFP and mCh-VTI12, or the Golgi marker mCh-MEMB12, and the thresholded merged images used for colocalization analyses. Images were obtained from two fluorescent channels simultaneously at the cell cortex. (*B*) Percentage of overall TVA-GFP (light blue bar), *small*-TVA (gray bar), and *large*-TVA (dark blue bar) compartments that colocalize with the markers VHAa1-RFP, mCh-VTI12, and mCh-MEMB12 for at least five contiguous frames of live-cell imaging. Dynamic colocalization was measured in a minimum of 15 cells from at least three different seedlings (data are mean ± SEM). (Scale bars, 5 μm.)

colocalization criteria over five adjacent frames is shown in Fig. 5*B*. The quantification of the particles using this approach revealed that 84.6% of the *large*-TVA and 42.1% of *small*-TVA vesicles were associated with CESA6-containing complexes at the cell cortex (Fig. 5*C* and Movie S9).

The observed localization of tdT-CESA6 to small compartments labeled by TVA-GFP was intriguing, as the molecular composition of the mobile vesicles carrying CSCs to the PM remains uncharacterized. To examine further these small compartments, we imaged cells in etiolated hypocotyls of the dual-labeled tdT-CESA6 and TVA-GFP line with spinning disk confocal microscopy, as tdT-CESA6 signal to noise and photobleaching were both high with the point scanning microscope used previously. We confirmed that both proteins colocalize to a subset of small-TVA compartments, although TVA-GFP is present in other small compartments not labeled by tdT-CESA6 (Fig. 6*A*). Thus, we hypothesized that TVA may be present in the vesicles delivering CSCs to the cell membrane. To test this idea, we photobleached tdT-CESA6 at the PM to clearly identify and quantify individual CSC delivery events in etiolated hypocotyls cells. Only after marking all such detectable CSC delivery events in each bleached area over a fixed time interval (between 150 and 240 s) was the TVA channel examined. We observed that punctate TVA-GFP signal was detected at the delivery site in 69 of 82 detected CESA delivery events (84.1%) (Fig. 6*B*). Additionally, in 53 of these events (76.8%), TVA-GFP was observed to dynamically colocalize with tdT-CESA6 vesicles prior to their stabilization at the delivery site (Fig. 6 *C* and *D*). Thus, TVA-GFP was detected at the majority of CSC delivery sites, where it was frequently observed to be associated with CSC secretory vesicles prior to their arrival at the PM (more examples shown in *SI Appendix*, Fig. S7). Both the mobile and the static TVA-GFP signals were consistent with *small*-TVA, indicating that at least some *small*-TVA may be secretory vesicles. Labeled TVA did not remain at the delivery site but disappeared soon after vesicle stabilization. Intriguingly, in 56.5% of the delivery events where TVA-GFP was detected, the label was also observed to move away from the delivery site as a discrete particle after CESA6 signal was positionally stabilized (*SI Appendix*, Fig. S8). TVA-GFP particles remained for a mean of 6.3 ± 0.42 s at the delivery site after observation of CESA6 stabilization (inferred to represent tethering) at the PM (Fig. 6*E*). Taken together, these data support the hypothesis that TVA protein plays a role in the delivery of CSCs to the PM, either in mediating progression of secretion at the TGN or facilitating final delivery to the PM (or possibly both).

In order to study whether TVA protein was more generally involved in the secretion pathway, we examined the distribution of two other PM proteins, PIN1-GFP and PEN3-GFP (45–47), in the *tva-1* mutant background. This analysis showed no significant change in the polar localization or intensity of these proteins

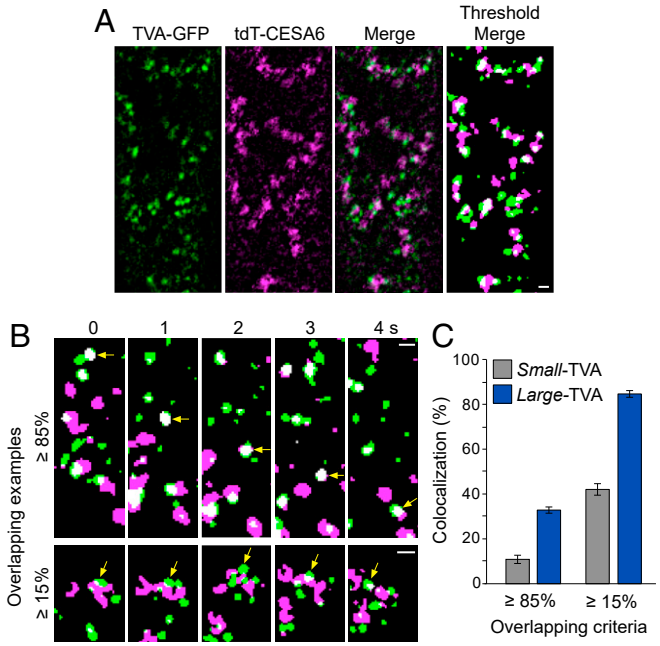


**Fig. 5.** TVA is associated with CESA complexes in the secretion pathway. (*A*) Single-frame images of 3-d-old etiolated hypocotyl cells expressing TVA-GFP and tdTomato-CESA6 (tdT-CESA6), and the thresholded merged images used for colocalization analyses. TVA-GFP and tdT-CESA6 were imaged simultaneously at the cell cortex focal plane. (*B*) Consecutives frames of a thresholded merged time series showing a representative example of each overlapping criteria (≥85% or ≥15%) used for the dynamic colocalization between TVA-GFP and tdT-CESA6. Colocalization events are indicated by yellow arrows. (*C*) Percentage of *small*-TVA (gray bars) and *large*-TVA (blue bars) compartments that colocalize with tdT-CESA6, for at least five contiguous frames, according to two different overlapping criteria. Data are means (± SEM) of $n = 24$ cells from six different seedlings. (Scale bars, 1 μm.)

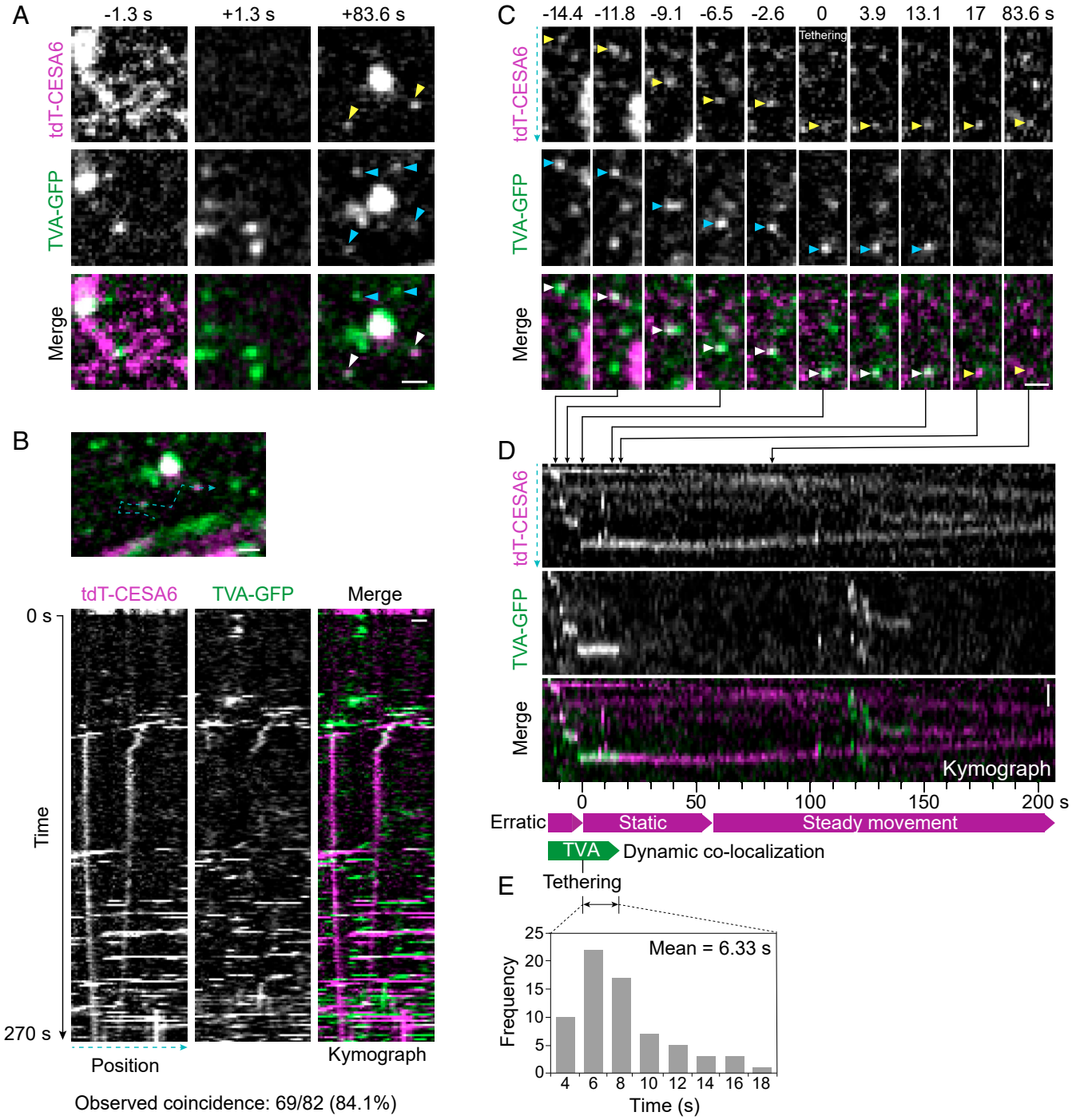


**Fig. 6.** TVA is associated with CESA complexes during their delivery at the PM. Etiolated hypocotyl cells expressing tdT-CESA6 and TVA-GFP were imaged at 1.3-s intervals after photobleaching tdTomato signal at the PM by spinning disk confocal microscopy. (*A*) Photobleaching was used to visualize small delivery vesicles for tdT-CESA6 complexes at the PM (yellow arrowhead). TVA-GFP (cyan arrowhead) colocalizes to the same small compartments (white arrowhead), although present in other small compartments not labeled by tdT-CESA6 as well. (*B*) Two tdT-CESA6 delivery events at the PM, and the coincident TVA-GFP, are seen on the kymograph taken along its path of movement (cyan line). TVA-GFP is present in 69 of 82 CESA delivery events (84.1%) analyzed in 40 cells from 17 seedlings. TVA-GFP colocalizes with tdT-CESA6 at the delivery sites at a frequency significantly higher than chance ($P < 0.001$, binomial test). (*C*) Time-lapse image series of a tdT-CESA6 complex delivery event. A tdT-CESA6 (yellow arrowhead) and TVA-GFP (cyan arrowhead) dynamically colocalize at the focal plane (white arrowhead) until the CESA particle is stabilized and tethered to the PM. TVA-GFP stays at the delivery site after tdT-CESA6 stabilization and then disappears. (*D*) Kymograph taken along the cyan trace in *C*. The tdT-CESA6 particle moves erratically at the focal plane, stabilizes for 56 s (static phase), and then starts moving at constant velocity (steady movement phase). The TVA-GFP particle is coincident with tdT-CESA6 during the erratic phase and stays at the delivery site during the static phase for 15 s before disappearing. *Bottom*: Schematic of the three stages of behavior of the CESA6 complex delivery event and TVA-GFP dynamic colocalization during the event. (*E*) Histogram showing the time TVA-GFP particles stay at delivery sites after tdT-CESA6 is tethered to the PM. (Scale bars, 1 μm.)

compared with wild type (*SI Appendix*, Fig. S9). However, this result does not preclude that TVA functions in secretion of other secretory cargos, a possibility suggested by the observation that TVA-GFP labels many compartments that are not clearly labeled by tdT-CESA6. Further studies will be required to assess the specificity of TVA for CSC secretion.

## Discussion

Cellulose is the principal component of plant cell walls; however, very little is known about how the CSCs are trafficked and delivered to the PM to initiate cellulose synthesis. In this study, we described TVA, a previously uncharacterized protein that is localized in at least two different intracellular trafficking compartments, and disruption of which leads to an increased sensitivity to cellulose synthesis inhibition, reduced cellulose content, and defective density and secretion of CSCs to the PM.

The reduction of cellulose content and sensitivity to cellulose inhibition in the *tva-1* mutant was not explained well by a role of TVA in promoting CSC activity. The analysis of GFP-CESA3 velocity at the PM in the *tva-1* mutant revealed a higher mean velocity of labeled CSCs compared with wild type, consistent with higher, and not lower biosynthetic activity of individual complexes (15, 32). However, we found that fewer CSCs were secreted to the PM and were significantly less dense in the *tva-1* mutant than in wild type, defects that would explain the increased sensitivity to isoxaben and DCB, and the reduced cellulose content in the mutant, and suggest a role of TVA in CSCs trafficking. The possible role of TVA in the secretion pathway was supported by the colocalization of these particles with the lipophilic probe FM4-64, the sensitivity to the exocytosis inhibitor BFA, and by the colocalization of *large*-TVA-GFP with markers of the TGN. Finally, we found that TVA protein colocalizes with CESA6 proteins at the TGN compartment and also at the secretory vesicles that deliver CSCs to the PM. Together, these data indicate that TVA acts to promote CSCs trafficking to the PM, likely acting to facilitate departure from the TGN or interaction of CSC secretory vesicles with the PM, or possibly both.

Why does loss of TVA function appear to result in increased synthesis by individual CSCs while total cellulose content is reduced? One reasonable possibility is that the reduced density of CSCs at the PM in the *tva* mutant results in the substrate being less limited because there are fewer CSCs competing for a common pool of UDP-glucose. Greater substrate availability may drive higher rates of synthesis, and thus motility of individual CSCs, despite an overall diminishment in synthesis. In fact, if the mean observed CSC velocities in hypocotyl epidermal cells are multiplied by the mean observed CSC densities, the total CSC synthetic output in the *tva-1* mutant is estimated to be 15% lower than that in wild type, in remarkable agreement with the measured 15% reduction in cellulose content in hypocotyls and leaves.

In our colocalization analysis between TVA and CESA6, we observed that some *large*-TVA-GFP particles partially overlapped with large tdT-CESA6–labeled compartments similar in size and morphology with previously described CESA-containing Golgi bodies (15, 18). The identity of these TVA-associated compartments as Golgi bodies was supported further by our independent observation of a similar association between *large*-TVA-GFP and the Golgi labeled with mCherry-MEMB12. Given that *large*-TVA compartments were labeled by TGN markers, these observations of a close and dynamic association between some *large*-TVA compartments and Golgi bodies are consistent with previous observations that TGN can show dynamic localization with the Golgi in higher plants (20, 43, 44). Therefore, the partial overlap of the TVA signal with large CESA6- or MEMB12-labeled Golgi likely results from close organelle association, and the TGN may be the first compartment in the secretory pathway where CSCs and TVA meet.

We found that TVA-GFP was present on the vesicles delivering CSCs to the PM, and both particles seem to move together prior to arrival at the PM. Thus, TVA is a marker for the "mobile" vesicles that deliver CSCs to the PM. Exocyst complex and the protein PATROL1 have been shown recently to be present at the delivery site, but at a later stage during the tethering of CSCs (26). After the secretion of CSCs at the PM, we observed *small*-TVA moving away from the delivery site as a discrete particle in 56% of the deliveries. This behavior resembles a kiss-and-run vesicle fusion event, such as described in the exocytosis of synaptic vesicles, where the delivering vesicle can be reused after the secretion (48).

The exact role of TVA in the secretory pathway and delivery of CSCs to the PM is unclear since it is a previously uncharacterized protein. TVA has a plant-specific DUF1218 domain of about 100 amino acids with several conserved Cys residues, which is present in a wide range of land plants, including liverworts, mosses, lycophytes, gymnosperms, monocots, and dicots (*SI Appendix*, Fig. S2*A*) but not in animal or fungal lineages, indicating that the TVA family might have a plant-specific function in vesicle trafficking.

An *Arabidopsis* homolog of *TVA*, At4g27435 (*TVL2*), was identified previously as one of the genes coregulated transcriptionally with secondary *CESAs*, with a potential function in cell wall synthesis (49). This gene, together with *TVA*, were also found to be the closest orthologs to a poplar gene, *PttUNKA*, that is expressed during secondary cell wall formation. Both *Arabidopsis* genes are expressed in secondary thickened hypocotyl tissue (50). However, while *TVL2* is more limited to stems, *TVA* is expressed in the majority of plant organs (50), as we also saw in our analyses (*SI Appendix*, Fig. S1), suggesting a more general role for TVA in both primary and secondary cell wall synthesis. Such a role would explain the reduction of cellulose not only in primary cell walls of seedlings, hypocotyls, and leaves, but also in the secondary cell wall of stems in the *tva-1* mutant.

Besides *TVL2*, there are five additional genes homologous to *TVA* in the *Arabidopsis* genome (*SI Appendix*, Fig. S2*A*) that might contribute redundantly to primary cell wall synthesis. This may account for the relative mild phenotype of *tva* mutants in cellulose synthesis. Further characterization of multiple knockout mutants in these genes would provide a more complete picture about the importance of this family to cell wall trafficking.

The functional characterization of the *TVA* gene, identified by a *CESA* coexpression approach, has demonstrated its involvement in the cellulose synthesis process, and specifically in the secretion pathway of the CSCs from the Golgi to the PM. Further analyses of the function of the protein will be required to gain insight into the specific role of TVA in this process. Understanding the molecular function of TVA, as well as identifying and characterizing new components from the compartments that regulate CSC trafficking, will provide important insights into the mechanism of CSC secretion and recycling, and their role in regulating cellulose synthesis, cell wall assembly, and plant growth.

## Materials and Methods

**Plant Material and Growth Conditions.** *A. thaliana* (Col-0) T-DNA insertion lines for *tva-1* (SALK_129213) and *tva-2* (GABI_256D04) were obtained from the *Arabidopsis* Biological Resource Center (ABRC) (51, 52). Primers used for molecular genotyping are listed in *SI Appendix*, Table S2. The marker lines GFP-CESA3 (7), tdTomato-CESA6 (24), VHAa1-RFP (41), mCherry-VTI12 and mCherry-MEMB12 (42), PIN1-GFP (45), and PEN3-GFP (46) have been described previously.

*Arabidopsis* seeds were sterilized with household bleach, washed with water, and stratified for 3 d at 4 °C in the dark. The seeds were germinated and grown vertically on Murashige and Skoog (MS) plates (one-half-strength MS salts, 1% sucrose, 0.9% agar, and 0.05% 2-(N-morpholino)ethanesulfonic acid (MES), pH 5.7) at 22 °C in long-day conditions (16-h light and 8-h dark cycle) or dark. For dark-grown seedlings, plates were previously exposed to ambient light for 3 h to induce germination and then transferred to dark. For drug treatments, the seeds were directly grown on plates supplemented with various amounts of isoxaben or DCB (Sigma) as indicated in figures and text.

**qRT-PCR.** For all the qRT-PCR experiments, three biological replicates and three technical replicates per sample were used. Total RNA was isolated from 9-d-old seedlings, 5-d-old etiolated hypocotyls, 4-wk-old leaves, stems, flowers, and siliques. Primers are listed in *SI Appendix*, Table S2.

**Constructs.** For the *TVA* promoter-GUS fusion construct, a 1,457-bp fragment upstream of the ATG of *TVA* was used. For the TVA-GFP fusion construct, a *TVA* genomic sequence, including the promoter and a 1,175-bp coding sequence, was used.

**Drug Treatments and FM4-64 Staining.** For drug treatments and FM4-64 staining, 3-d-old etiolated seedlings were incubated in 2 mL of liquid MS containing either 1 μM LatB, 20 μM Oryzalin, or 50 μM BFA (Sigma-Aldrich) for the indicated times before imaging. Endocytosis and colocalization studies were performed with 4 μM FM4-64. Control treatments were performed with equal amounts of the respective solvents (dimethyl sulfoxide (DMSO) or ethanol).

See *SI Appendix, SI Materials and Methods* for a detailed description of the experimental procedures.

**Data Availability.** All study data are included in the article and/or supporting information.

**ACKNOWLEDGMENTS.** We thank C.R.S., D.W.E., and J.R.D. laboratory members for helpful discussions and review of the manuscript. We thank Heather Cartwright from the imaging facility of Carnegie Institution for her technical assistance with the microscopes. We also thank ABRC for providing the T-DNA lines. T.V. was supported by an European Molecular Biology Organization (EMBO) long-term fellowship (ALTF 711-2012) and by post-doctoral funding from the Philomathia Foundation. This work was supported by the Energy Bioscience Institute, Carnegie Institution for Science, and NIH National Institute of General Medical Sciences (NIGMS) (R01 GM123259-01).

1. C. Somerville *et al*., Toward a systems approach to understanding plant cell walls. *Science* **306**, 2206–2211 (2004).
2. E. R. Lampugnani, G. A. Khan, M. Somssich, S. Persson, Building a plant cell wall at a glance. *J. Cell Sci.* **131**, 10.1242/jcs.207373 (2018).
3. H. E. McFarlane, A. Döring, S. Persson, The cell biology of cellulose synthesis. *Annu. Rev. Plant Biol.* **65**, 69–94 (2014).
4. J. J. Kieber, J. Polko, The regulation of cellulose biosynthesis in plants. *Plant Cell* **31**, 282–296 10.1105/tpc.18.00760. (2019).
5. C. Somerville, Cellulose synthesis in higher plants. *Annu. Rev. Cell Dev. Biol.* **22**, 53–78 (2006).
6. N. G. Taylor, R. M. Howells, A. K. Huttly, K. Vickers, S. R. Turner, Interactions among three distinct CesA proteins essential for cellulose synthesis. *Proc. Natl. Acad. Sci. U.S.A.* **100**, 1450–1455 (2003).
7. T. Desprez *et al*., Organization of cellulose synthase complexes involved in primary cell wall synthesis in Arabidopsis thaliana. *Proc. Natl. Acad. Sci. U.S.A.* **104**, 15572–15577 (2007).
8. S. Persson *et al*., Genetic evidence for three unique components in primary cell-wall cellulose synthase complexes in Arabidopsis. *Proc. Natl. Acad. Sci. U.S.A.* **104**, 15566–15571 (2007).
9. L. Liu *et al*., Brittle Culm1, a COBRA-like protein, functions in cellulose assembly through binding cellulose microfibrils. *PLoS Genet.* **9**, e1003704 (2013).
10. T. Vain *et al*., The cellulase KORRIGAN is part of the cellulose synthase complex. *Plant Physiol.* **165**, 1521–1532 (2014).
11. Y. Gu *et al*., Identification of a cellulose synthase-associated protein required for cellulose biosynthesis. *Proc. Natl. Acad. Sci. U.S.A.* **107**, 12866–12871 (2010).
12. M. Bringmann *et al*., POM-POM2/cellulose synthase interacting1 is essential for the functional association of cellulose synthase and microtubules in Arabidopsis. *Plant Cell* **24**, 163–177 10.1105/tpc.111.093575. (2012).
13. S. Li, L. Lei, C. R. Somerville, Y. Gu, Cellulose synthase interactive protein 1 (CSI1) links microtubules and cellulose synthase complexes. *Proc. Natl. Acad. Sci. U.S.A.* **109**, 185–190 (2012).
14. A. Endler *et al*., A mechanism for sustained cellulose synthesis during salt stress. *Cell* **162**, 1353–1364 (2015).
15. A. R. Paredez, C. R. Somerville, D. W. Ehrhardt, Visualization of cellulose synthase demonstrates functional association with microtubules. *Science* **312**, 1491–1495 (2006).
16. C. H. Haigler, R. M. Brown, Transport of rosettes from the golgi apparatus to the plasma membrane in isolated mesophyll cells of Zinnia elegans during differentiation to tracheary elements in suspension culture. *Protoplasma* **134**, 111–120 (1986).
17. E. F. Crowell *et al*., Pausing of Golgi bodies on microtubules regulates secretion of cellulose synthase complexes in Arabidopsis. *Plant Cell* **21**, 1141–1154 (2009).
18. R. Gutierrez, J. J. Lindeboom, A. R. Paredez, A. M. Emons, D. W. Ehrhardt, Arabidopsis cortical microtubules position cellulose synthase delivery to the plasma membrane and interact with cellulose synthase trafficking compartments. *Nat. Cell Biol.* **11**, 797–806 (2009).
19. Y. Zhang *et al*., Golgi-localized STELLO proteins regulate the assembly and trafficking of cellulose synthase complexes in Arabidopsis. *Nat. Commun.* **7**, 1–14 (2016).
20. C. Viotti *et al*., Endocytic and secretory traffic in Arabidopsis merge in the trans-Golgi network/early endosome, an independent and highly dynamic organelle. *Plant Cell* **22**, 1344–1357 (2010).
21. M. R. Rosquete, D. J. Davis, G. Drakakaki, The plant trans-Golgi network: Not just a matter of distinction. *Plant Physiol.* **176**, 187–198 (2018).
22. G. Drakakaki *et al*., Isolation and proteomic analysis of the SYP61 compartment reveal its role in exocytic trafficking in Arabidopsis. *Cell Res.* **22**, 413–424 (2012).
23. S. J. Kim, F. Brandizzi, The plant secretory pathway: An essential factory for building the plant cell wall. *Plant Cell Physiol.* **55**, 687–693 (2014).
24. A. Sampathkumar *et al*., Patterning and lifetime of plasma membrane-localized cellulose synthase is dependent on actin organization in Arabidopsis interphase cells. *Plant Physiol.* **162**, 675–688 (2013).
25. W. Zhang, C. Cai, C. J. Staiger, Myosins XI are involved in exocytosis of cellulose synthase complexes. *Plant Physiol.* **179**, 1537–1555 (2019).
26. X. Zhu, S. Li, S. Pan, X. Xin, Y. Gu, CSI1, PATROL1, and exocyst complex cooperate in delivery of cellulose synthase complexes to the plasma membrane. *Proc. Natl. Acad. Sci. U.S.A.* **115**, E3578–E3587 10.1073/pnas.1800182115 (2018).
27. J. K. Polko *et al*., SHOU4 proteins regulate trafficking of cellulose synthase complexes to the plasma membrane. *Curr. Biol.* **28**, 3174–3182.e6 (2018).
28. M. Mutwil, J. Obro, W. G. Willats, S. Persson, GeneCAT—novel webtools that combine BLAST and co-expression analyses. *Nucleic Acids Res.* **36**, W320–W326 (2008).
29. R. Schwacke *et al*., ARAMEMNON, a novel database for Arabidopsis integral membrane proteins. *Plant Physiol.* **131**, 16–26 (2003).
30. C. Sánchez-Rodríguez *et al*., Chitinase-like1/pom-pom1 and its homolog CTL2 are glucan-interacting proteins important for cellulose biosynthesis in Arabidopsis. *Plant Cell* **24**, 589–607 (2012).
31. A. Caño-Delgado, S. Penfield, C. Smith, M. Catley, M. Bevan, Reduced cellulose synthesis invokes lignification and defense responses in Arabidopsis thaliana. *Plant J.* **34**, 351–362 (2003).
32. S. DeBolt, R. Gutierrez, D. W. Ehrhardt, C. Somerville, Nonmotile cellulose synthase subunits repeatedly accumulate within localized regions at the plasma membrane in Arabidopsis hypocotyl cells following 2,6-dichlorobenzonitrile treatment. *Plant Physiol.* **145**, 334–338 (2007).
33. T. Vellosillo, T. Yeats, N. Sorek, Analysis of in vivo cellulose biosynthesis in Arabidopsis cells by spinning disk confocal microscopy. *Bio Protoc.* **5**, e1617 (2015).
34. T. Shimmen, E. Yokota, Cytoplasmic streaming in plants. *Curr. Opin. Cell Biol.* **16**, 68–72 (2004).
35. D. Szymanski, C. J. Staiger, The actin cytoskeleton: Functional arrays for cytoplasmic organization and cell shape control. *Plant Physiol.* **176**, 106–118 (2018).
36. S. DeBolt *et al*., Morlin, an inhibitor of cortical microtubule dynamics and cellulose synthase movement. *Proc. Natl. Acad. Sci. U.S.A.* **104**, 5854–5859 (2007).
37. A. Nebenführ, C. Ritzenthaler, D. G. Robinson, Brefeldin A: deciphering an enigmatic inhibitor of secretion. *Plant Physiol.* **130**, 1102–1108 (2002).
38. N. Geldner *et al*., The Arabidopsis GNOM ARF-GEF mediates endosomal recycling, auxin transport, and auxin-dependent plant growth. *Cell* **112**, 219–230 (2003).
39. A. A. Sanderfoot, V. Kovaleva, D. C. Bassham, N. V. Raikhel, Interactions between syntaxins identify at least five SNARE complexes within the Golgi/prevacuolar system of the Arabidopsis cell. *Mol. Biol. Cell* **12**, 3733–3743 (2001).
40. T. Uemura *et al*., Systematic analysis of SNARE molecules in Arabidopsis: dissection of the post-Golgi network in plant cells. *Cell Struct. Funct.* **29**, 49–65 (2004).
41. J. Dettmer, A. Hong-Hermesdorf, Y. D. Stierhof, K. Schumacher, Vacuolar H+-ATPase activity is required for endocytic and secretory trafficking in Arabidopsis. *Plant Cell* **18**, 715–730 (2006).
42. N. Geldner *et al*., Rapid, combinatorial analysis of membrane compartments in intact plants with a multicolor marker set. *Plant J.* **59**, 169–178 (2009).
43. T. Uemura, Y. Suda, T. Ueda, A. Nakano, Dynamic behavior of the trans-golgi network in root tissues of Arabidopsis revealed by super-resolution live imaging. *Plant Cell Physiol.* **55**, 694–703 (2014).
44. J. A. Sparks *et al*., HLB1 is a tetratricopeptide repeat domain-containing protein that operates at the intersection of the exocytic and endocytic pathways at the TGN/EE in Arabidopsis. *Plant Cell* **28**, 746–769 (2016).
45. E. Benková *et al*., Local, efflux-dependent auxin gradients as a common module for plant organ formation. *Cell* **115**, 591–602 (2003).
46. M. Stein *et al*., Arabidopsis PEN3/PDR8, an ATP binding cassette transporter, contributes to nonhost resistance to inappropriate pathogens that enter by direct penetration. *Plant Cell* **18**, 731–746 (2006).
47. L. Langowski, K. Rüzicka, S. Naramoto, J. Kleine-Vehn, J. Friml, Trafficking to the outer polar domain defines the root-soil interface. *Curr. Biol.* **20**, 904–908 (2010).
48. A. A. Alabi, R. W. Tsien, Perspectives on kiss-and-run: Role in exocytosis, endocytosis, and neurotransmission. *Annu. Rev. Physiol.* **75**, 393–422 (2013).
49. S. Persson, H. Wei, J. Milne, G. P. Page, C. R. Somerville, Identification of genes required for cellulose synthesis by regression analysis of public microarray data sets. *Proc. Natl. Acad. Sci. U.S.A.* **102**, 8633–8638 (2005).
50. S. Ubeda-Tomas *et al*., Genomic-assisted identification of genes involved in secondary growth in Arabidopsis utilising transcript profiling of poplar wood-forming tissues. *Physiol. Plant.* **129**, 415–428 (2007).
51. J. M. Alonso *et al*., Genome-wide insertional mutagenesis of Arabidopsis thaliana. *Science* **301**, 653–657 (2003).
52. N. Kleinboelting, G. Huep, A. Kloetgen, P. Viehoever, B. Weisshaar, GABI-Kat SimpleSearch: new features of the Arabidopsis thaliana T-DNA mutant database. *Nucleic Acids Res.* **40**, D1211–D1215 (2012).